Ultranarrow bandwidth tunable atomic filter via quantum interference-induced polarization rotation in Rb vapor

Zheng Tan (谭 政)[1,2], Xianping Sun (孙献平)[1*], Jun Luo (罗 军)[1,2], Yong Cheng (程 雍)[1,2], Xiuchao Zhao (赵修超)[1], Xin Zhou (周 欣)[1], Jin Wang (王 谨)[1,2], and Mingsheng Zhan (詹明生)[1,2]**

[1]*State Key Laboratory of Magnetic Resonance and Atomic and Molecular Physics, Wuhan Institute of Physics and Mathematics, Chinese Academy of Sciences – Wuhan National Laboratory for Optoelectronics, Wuhan 430071, China*

[2]*Center for Cold Atom Physics, Chinese Academy of Sciences, Wuhan 430071, China*

[*]*Corresponding author: xpsun@wipm.ac.cn;* [**]*corresponding author: mszhan@wipm.ac.cn*

Received August 5, 2014; accepted October 24, 2014; posted online November 28, 2014

We report the experimental demonstration of an ultranarrow bandwidth atomic filter by optically induced polarization rotation in multilevel electromagnetically induced transparency systems in hot Rb vapor. With a coupling intensity of 2.3 W/cm^2, the filter shows a peak transmission of 33.2% and a bandwidth of 10 MHz. By altering the coupling frequency, a broad tuning range of several Doppler linewidths of the D1 line transitions of ^{87}Rb atoms can be obtained. The presented atomic filter has useful features of ultranarrow bandwidth, and the operating frequency can be tuned resonance with the atomic transition. Such narrowband tunable atomic filter can be used as an efficient noise rejection tool in classical and quantum optical applications.

OCIS codes: 140.0140, 020.1670, 300.6210.
doi: 10.3788/COL201412.121404.

Narrowband optical filter is an essential tool to extract useful signals from a noisy background. Different approaches have been used to achieve a narrowband optical filter, such as multiple cavity optical filters[1,2], microresonator filters[3], filters based on stimulated Brillouin scattering in optical fibers[4], and atomic filters[5]. Atomic filters based on magneto-optic effects[6] have been studied extensively, with the merits of narrow bandwidth, high transmission, and excellent noise rejection ability. For example, the Faraday anomalous dispersion optical filter[7,8], which has been demonstrated in Rb, Cs, Na, Ca, and K, and further been applied in the areas of laser communications[9], LIDAR[10], and quantum key distributions[11]. For a typical atomic filter, an externally applied electric field either longitudinal (the Faraday effect)[12] or transverse (the Voigt effect)[13] is introduced to cause the polarization rotation of the linearly polarized light by the large dispersion of the Faraday effect in the vicinity of the atomic resonance. Besides, the polarization rotation of the polarized light generated by laser-induced circular birefringence or dichroism of the medium via optical pumping among the energy sub-levels[14–16] or resonant two-photon process in an atomic system[17–21] has been demonstrated in either hot atomic vapor or cold atoms.

Atomic filter whose bandwidth is approaching atomic natural linewidth is essential for quantum information applications. It has been demonstrated that the atomic filter is an efficient tool for noise rejection in quantum key distributions[11], sub-Doppler bandwidth atomic filter with nonlinear optical amplification has been realized for further improving the signal-to-noise ratio in weak signal detection[22]. Recently, narrowband photon sources as one of the key components for quantum communications have attracted a great deal of interest. However, the bandwidth of the single photon generated by spontaneously parametric down-conversion in the nonlinear crystal[23] is usually very broad. In order to efficiently couple to atomic-ensemble-based quantum memories, a narrowband filter is required to fit for the atomic natural linewidth which is typically of the order of several megahertz for alkali vapors.

In this letter, we report the experimental realization of an ultranarrow bandwidth atomic filter in hot Rb vapor by using quantum interference-induced polarization rotation. The atomic filter presented here reveals a much narrower bandwidth which approaches the natural linewidth of Rb atoms. Moreover, a relatively higher peak transmission is obtained, owing to both large optical polarization rotation achieved in this system and low loss for the probe laser under conditions of electromagnetically induced transparency (EIT). We also demonstrated the frequency tunability of the filter by altering the coupling frequency. In particular, the center frequency of the filter can be tuned on resonance with the atomic transition, a favorable feature in atomic and quantum optics applications in comparison with dispersive atomic filters whose working frequency is far from atomic resonance.

EIT[24] is a quantum coherence and interference phenomenon, it can render an atomic medium almost transparency to the probe light while generating a large

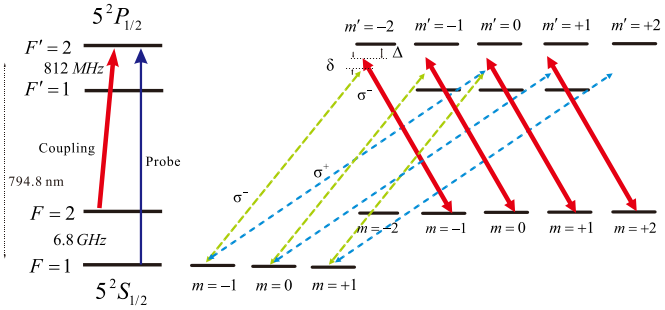

Fig. 1. Relevant energy levels of the D1 line transitions of ^{87}Rb atoms. The right-hand circularly (σ^-) polarized coupling laser (solid red lines) drives $5^2S_{1/2}$ $(F=2)\rightarrow 5^2P_{1/2}$ $(F'=2)$ transition. The probe laser containing equal parts of the right-hand circularly (σ^-) (dashed green lines) and left-hand circularly (σ^+) (dashed blue lines) polarized components is tuned on resonance with the $5^2S_{1/2}$ $(F=1)\rightarrow 5^2P_{1/2}$transition. Δ is the single photon detuning between states $5^2S_{1/2}$ $(F=2)$ and $5^2P_{1/2}$ $(F'=2)$ and δ is the two-photon detuning between states $5^2S_{1/2}$ $(F=1)$ and $5^2S_{1/2}$ $(F=2)$.

dispersion in a narrow window near the atomic resonance. EIT offers an efficient means of modifying optical properties of the atomic medium, which can be used to reduce the linear absorption and meanwhile dramatically enhance nonlinearities of the atomic medium. The nonlinear Faraday effect under conditions of EIT has been studied[25], where the polarization rotation was greatly reduced at the two-photon resonance. In the following, we demonstrate the enhancement of polarization rotation induced by quantum interference in the multilevel EIT systems. By utilizing the features of narrow linewidth and absorption reduction of EIT, an ultranarrow bandwidth atomic filter with relative high transmission can be realized with properly choosing atomic transitions and light polarization.

The energy levels used in our experiment is shown in Fig. 1. In a Λ-type configuration of ^{87}Rb atoms, the right-hand circularly (σ^-) polarized coupling laser interacts with the ground state $5^2S_{1/2}(F=2)$ and the excited state $5^2P_{1/2}(F'=2)$, and the linearly polarized probe laser (consisting of σ^+ and σ^- polarized components with equal amounts) drives the $5^2S_{1/2}(F=1)\rightarrow 5^2P_{1/2}$ transition. The different dispersive characters of σ^+ and σ^- components under the action of the coupling light cause different susceptibilities of the two polarized components. The incident linearly polarized probe laser can be expressed as[26]

$$E_{\text{in}} = \frac{1}{\sqrt{2}} E_0 \left[\hat{e}_+ e^{ik_+ z} + \hat{e}_- e^{ik_- z}\right] e^{-i\omega t}, \quad (1)$$

where $\hat{e}_+$ and $\hat{e}_-$ are σ^+ and σ^- polarized modes, respectively, and k_+ and k_- are complex wave numbers. After the probe laser passing through a Rb vapor cell sandwiched between two crossed polarizers, the probe transmission is given as

$$T = \frac{1}{2}\exp\left[-\frac{\omega l}{2c}\text{Im}(\chi_+ + \chi_-)\right] \times\left\{\cosh\left[\frac{\omega l}{2c}\text{Im}(\chi_+ - \chi_-)\right] - \cos\left[\frac{\omega l}{2c}\text{Re}(\chi_+ - \chi_-)\right]\right\}, \quad (2)$$

where χ_- and χ_+ are the total susceptibilities for σ^+ and σ^- polarized components of the probe laser, respectively, and l is the length of the Rb vapor cell.

According to Eq. (2), in the absence of the coupling laser, there is no difference between χ_- and χ_+, thus the background noise is rejected by the two crossed polarizers, and the probe transmission should be zero. While in the presence of the circularly polarized coupling laser, the quantum interference-induced anisotropy in the atomic medium causes $\chi_+ \neq \chi_-$, as the probe laser beam passes through the atomic medium, the plane of polarization will rotate an angle within the EIT window as a result of different susceptibilities of σ^+ and σ^- polarized components. Thus, the function of an ultranarrow bandwidth filter can be achieved in the multilevel EIT systems.

The experimental schematic is shown in Fig. 2. Two external cavity diode lasers at wavelength of 795 nm are used as the probe and the coupling laser, respectively. A 100 mm long natural abundance Rb vapor cell (Rb cell 2) with a magnetic shielding is temperature stabilized to 342 K, corresponding to the atomic density of 6.2×10^{11}cm^{-3}, and the diameter of the cell is 25 mm. The probe laser is linearly polarized and its frequency is scanned over a range of ~4 GHz around the $5^2S_{1/2}(F=1)\rightarrow 5^2P_{1/2}(F'=2)$ transition of ^{87}Rb atoms, and the coupling laser whose frequency is tuned to the $5^2S_{1/2}(F=2)\rightarrow 5^2P_{1/2}(F'=2)$ transition is set to right-hand circular (σ^-) polarization by using a half-wave plate (HWP2) and a quarter-wave plate (QWP2), a revised angular setting of these wave plates is adopted taking into consideration the imperfection of wave plates and polarization rotation introduced by mirrors reflection. The probe and coupling lasers co-propagate into the Rb vapor cell to form the Doppler-free configuration in the Λ-type system. In order to obtain a good spatial overlap in the cell, the probe and coupling laser beams have a small angle of about 5 mrad and the beam diameters are 0.5 and 1 mm, respectively. The probe laser beam passes through two crossed Glan–Thompson prisms (GT1 and GT2, with extinction ratios of 10^5:1) before reaching the photodiodes detector. An aperture (AP) is used to further eliminate the scattering of the coupling laser.

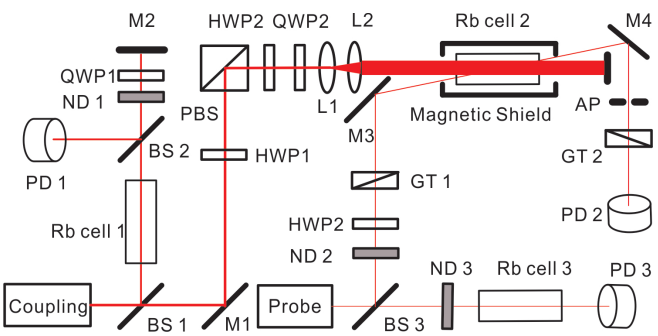

Fig. 2. Experimental schematic. PBS, polarizing beam splitter; M, mirror; ND, neutral-density filter; PD, photodiode detector; L, lens.

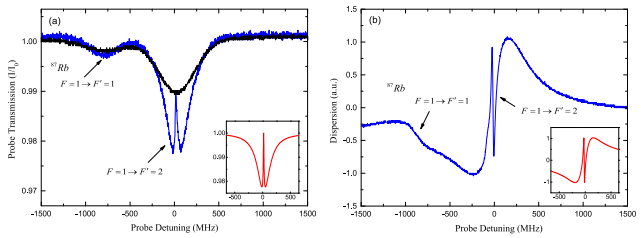

Fig. 3. Measured probe transmission and dispersion of the three-level atom versus the probe detuning: (a) transmission with no coupling laser (black curve) and with coupling laser on resonance (blue curve) and (b) dispersion with coupling laser on resonance (blue curve). The insets show theoretical plots of the transmission and dispersion curves (red curve) of the $5^2S_{1/2}$ $(F = 1) \rightarrow 5^2P_{1/2}$ $(F' = 2)$ transition at the two-photon resonance for reasonable parameter values.

Rb cell 3 is utilized to monitor the reference absorption spectroscopy of the probe, and Rb cell 1 is used as a frequency reference to calibrate the coupling detuning from the $5^2S_{1/2}$ $(F = 2) \rightarrow 5^2P_{1/2}$ $(F' = 2)$ transition. A digital oscilloscope is used to record the output from the detector.

The polarization of the probe laser is selected in the horizontal direction after passing through the GT1. In the presence of the σ^- polarized coupling laser, optical anisotropy is introduced into the atomic medium, if the probe laser is resonant with the $5^2S_{1/2}$ $(F = 1) \rightarrow 5^2P_{1/2}$ $(F' = 2)$ transition and satisfies two-photon resonance with the coupling laser $(\delta = 0)$, it experiences polarization rotation and passes the GT2. Otherwise, it is rejected by the crossed GTs.

Firstly, the probe transmission and dispersion spectrum of the three-level Λ-type atomic systems under conditions of EIT are measured. In Fig. 3(a), the increased absorption of the $5^2P_{1/2}(F' = 2)$ state when the coupling laser is tuned to the $5^2S_{1/2}(F = 2) \rightarrow 5^2P_{1/2}(F' = 2)$ transition is due to optical pumping of the coupling laser. As shown in Fig. 3(b), the steep dispersive curve indicates the rapid variation of the refractive index at the two-photon resonance. In the presence of the circularly polarized coupling laser, the differences in susceptibilities of the two circularly polarized components cause different dispersive and absorptive characters. The polarization rotation of the linear polarized probe light occurs near the two-photon resonance where EIT renders the atomic medium both anisotropic and transparency to the probe laser.

Figure 4 shows the transmission spectrum of the atomic filter when the coupling detuning is $\Delta = 230$ MHz with respect to the $5^2S_{1/2}(F = 2) \rightarrow 5^2P_{1/2}(F' = 2)$ resonance. The observed transmission peak is also located at $\delta = 230$ MHz detuned to the $5^2S_{1/2}(F = 1) \rightarrow 5^2P_{1/2}(F' = 2)$ resonance for the satisfactory of two-photon resonance $(\delta = 0)$. The measured filter bandwidth (the full-width at half-maximum of the transmission peak) is 10 MHz. The peak transmission is characterized as the ratio of the transmitted intensity (I) to that measured without the coupling laser and two GTs are set uncrossed (I_0). As

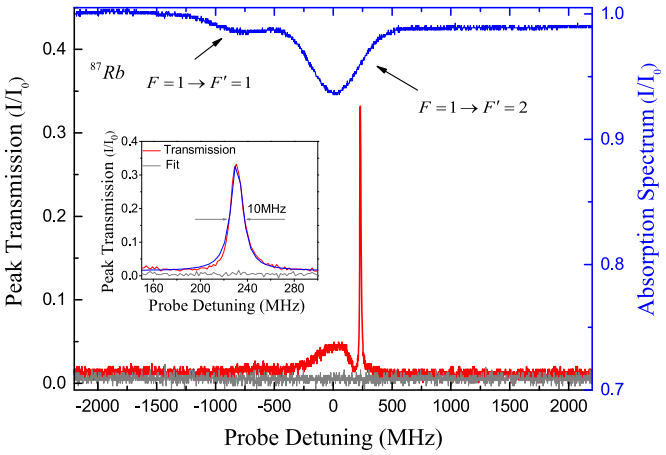

Fig. 4. Measured transmission spectrum of the filter (red curve) when the coupling intensity is 2.3 W/cm^2 and the temperature of the Rb vapor cell 2 is kept at 342 K. The bottom trace (gray curve) is the probe transmission without the coupling laser. The top trace (blue curve) is the reference Doppler absorption spectrum of the D1 line transitions of ^{87}Rb atoms. The inset shows the details of the transmission spectrum of the filter.

shown in Fig. 4, a maximum peak transmission of 33.2% is obtained with the coupling intensity of 2.3 W/cm^2 and the probe intensity of 0.28 mW/cm^2 at 342 K. In the absence of the coupling laser, the transmission spectrum of the filter disappears, and the same result also occurs when either of the probe laser and the coupling laser is tuned far-off resonance. The scattering of the coupling laser on the surface of the cell and collision-induced depolarization of the probe laser cause the baseline of the transmission spectrum slightly above zero. By using of a Fabry–Perot etalon before the photodiode detector 2, the physical nature of the detected signals can be approved exactly.

The center frequency of the filter can be tuned over several Doppler linewidths by altering the coupling frequency. As the coupling is far-off single-photon

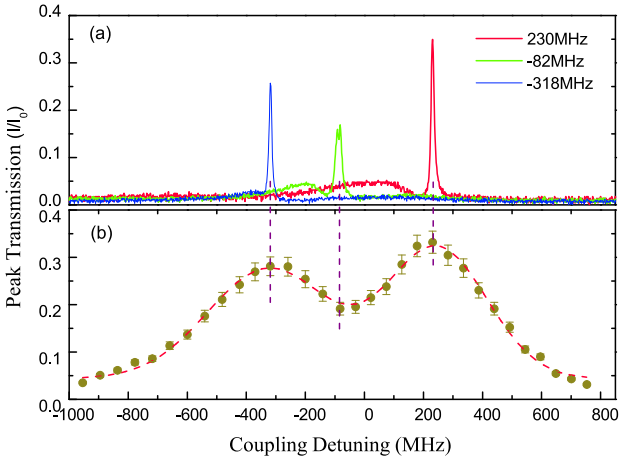

Fig. 5. (a) Transmission spectra of the filter when the detuning of the coupling laser are -318 MHz (blue trace), -82 MHz (green trace), and 230 MHz (red trace) and (b) peak transmission versus the detuning of the coupling laser.

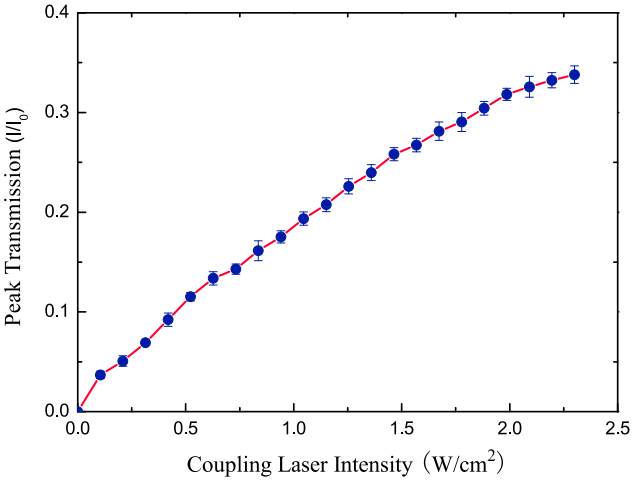

Fig. 6. Peak transmission of the filter as a function of coupling laser intensity at 342 K, the coupling detuning $\Delta = 230$ MHz.

resonance, the EIT line shape transforms into Raman absorption profile[27], in such case, the polarization rotation of the probe laser is due to $\chi_+ \neq \chi_-$ for σ^+ and σ^- polarized components in different Raman sub-transitions. Figure 5(b) shows the peak transmission of the filter as a function of the coupling detuning from the $5^2S_{1/2}(F=2) \rightarrow 5^2P_{1/2}(F'=2)$ resonance. Two maximum peaks on the transmission curve are located at $\Delta = -318$ and 230 MHz, respectively. The asymmetry of the transmission curve is due to the effect of the $5^2S_{1/2}(F=2) \rightarrow 5^2P_{1/2}(F'=1)$ transition, which also has a less efficient contribution to the polarization rotation of the probe laser when the coupling frequency is tuned nearby.

Figure 6 shows the variation of peak transmission with the coupling laser intensity. When the coupling laser intensity is below a certain level, higher coupling intensity will cause larger polarization rotation, and thus allows higher transmission efficiency. Then, the transmission saturates at large coupling laser intensity. In our experiment, the maximum transmission efficiency of 33.2% is measured with the coupling intensity of 2.3 W/cm^2.

In conclusion, we experimentally demonstrate an ultranarrow bandwidth atomic filter by using quantum interference of the EIT atomic system in Rb D1 line transition (795 nm). A maximum transmission of 33.2% is achieved with the coupling intensity of 2.3 W/cm^2. As an advantage of this atomic filter, the bandwidth is narrowed to 10 MHz, which is approaching the natural linewidth of Rb atoms. We realize the frequency tunability of the filter by altering the coupling frequency, with a fast and easy tunable feature. Such tunable atomic filter with an ultranarrow bandwidth can be a useful noise rejection tool and may find applications in a variety of classical and quantum optical applications. It is also particularly suitable for the generation of the single photon and atomic physics experiments, where a narrow bandwidth filter with passband matching atomic resonant frequency is required.

This work was supported by the National Basic Research Program of China (No. 2006CB921203), the National Natural Science Foundation of China (No. 11174327), and the Foundation of Wuhan National Laboratory for Optoelectronics (No. P080002). XZ thanks the support of the Hundred Talent Program by the Chinese Academy of Sciences.

References

1. W. Gunning, Appl. Opt. **21,** 3129 (1982).
2. Z. Chen, J. Chen, Y. Li, J. Qian, J. Qi, J. Xu, and Q. Sun, Chin. Opt. Lett. **11,** 112403 (2013).
3. C. Yin, J. Gu, M. Li, and Y. Song, Chin. Opt. Lett. **11,** 082302 (2013).
4. T. Tanemura, Y. Takushima, and K. Kikuchi, Opt. Lett. **27,** 1552 (2002).
5. P. Yeh, Appl. Opt. **21,** 2069 (1982).
6. D. Budker, W. Gawlik, D. F. Kimball, S. M. Rochester, V. V. Yashchuk, and A. Weis, Rev. Mod. Phys. **74,** 1153 (2002).
7. B. Yin and T. M. Shay, Opt. Lett. **20,** 1617 (1991).
8. Z. L. Hu, X. P. Sun, Y. P. Liu, L. P. Fu, and X. Z. Zeng, Opt. Commun. **156,** 289 (1998).
9. J. X. Tang, Q. J. Wang, Y. M. Li, L. Zhang, J. H. Gan, M. H. Duan, J. K. Kong, and L. M. Zheng, Appl. Opt. **34,** 2619 (1995).
10. J. Höffner and C. F. Begemann, Opt. Lett. **30,** 890 (2005).
11. X. Shan, X. P. Sun, J. Luo, Z. Tan, and M. S. Zhan, Appl. Phys. Lett. **89,** 191121 (2006).
12. Z. L. Lee, D. Heiman, H. Wang, C. G. Fonstad, M. Sundaram, and A. C. Gossard, Appl. Phys. Lett. **69,** 3731 (1996).
13. K. H. Drake, W. Lange, and J. Mlynek, Opt. Commun. **66,** 315 (1988).
14. L. D. Turner, V. Karaganov, P. J. O. Teubner, and R. E. Scholten, Opt. Lett. **27,** 500 (2002).
15. A. Cere, V. Parigi, M. Abad, F. Wolfgramm, A. Predojevic, and M. W. Mitchell, Opt. Lett. **34,** 1012 (2009).
16. Y. F. Wang, S. N. Zhang, D. Y. Wang, Z. M. Tao, Y. L. Hong, and J. B. Chen, Opt. Lett. **37,** 4059 (2012).
17. S. Wielandy and A. L. Gaeta, Phys. Rev. Lett. **81,** 3359 (1998).
18. J. Keaveney, A. Sargsyan, D. Sarkisyan, A. Papoyan, and C. S. Adams, J. Phys. B: At. Mol. Opt. Phys. **47,** 075002 (2014).
19. S. J. Li, B. Wang, X. D. Yang, Y. X. Han, H. Wang, M. Xiao, and K. C. Peng, Phys. Rev. A **74,** 033821 (2006).
20. J. M. Choi, J. M. Kim, Q. H. Park, and D. Cho, Phys. Rev. A **75,** 013815 (2007).
21. V. M. Datsyuk, I. M. Sokolov, and D. V. Kupriyanov, Phys. Rev. A **77,** 033823 (2008).
22. Z. Tan, X. Sun, J. Luo, Y. Cheng, J. Wang and M. Zhan, Chin. Opt. Lett. **9,** 021405 (2011).
23. B. S. Shi, F. Y. Wang, C. Zhai, and G. C. Guo, Opt. Commun. **281,** 3390 (2008).
24. S. E. Harris, Phys. Today **50,** 36 (1997).
25. R. Drampyan, S. Pustelny, and W. Gawlik, Phys. Rev. A **80,** 033815 (2009).
26. E. T. Dressler, A. E. Laux, and R. I. Billmers, J. Opt. Soc. Am. B **13,** 1849 (1996).
27. M. V. Pack, R. M. Camacho, and J. C. Howell, Phys. Rev. A **76,** 013801 (2007).